Oil & Gas Science and Technology – Rev. IFP Energies nouvelles **75**, 2 (2020)

https://doi.org/10.2516/ogst/2019068

Available online at:
ogst.ifpenergiesnouvelles.fr

REGULAR ARTICLE OPEN ACCESS

A relative permeability model for CBM reservoir

Zeyang Peng[1,2,*], Xiangfang Li[3], and Zheng Sun[3]

[1] SINOPEC Petroleum Exploration and Production Research Institute, 100083 Beijing, PR China
[2] SINOPEC Key Laboratory of Shale Oil/Gas Exploration & Production, 100083 Beijing, PR China
[3] Key Laboratory for Petroleum Engineering of the Ministry of Education, China University of Petroleum, 102249 Beijing, PR China

Received: 15 October 2018 / Accepted: 11 December 2019

Abstract. Relative permeability is an effective tool for studying multiphase fluid flow in porous media. For conventional reservoirs, a relatively reliable relative permeability curve can be obtained by laboratory core test. But because of the coalbed gas reservoir permeability is low, the stable steady state method will take a very long time, and the operation is relatively complex. For the non-steady state method, the coalbed gas reservoirs are rich in micro nano pore, which causes the strong heterogeneity and gas is easy to break in through the cracks, it makes non-steady displacement experiment very difficult. Also, the experimental results are greatly affected by human factors and computational methods. Therefore, based on the ideal pore structure and the consideration of different displacement mechanisms, the analytical method not only helps to understand the mechanism of gas water two-phase flow, but also is a convenient and practical method. Coalbed methane reservoirs are rich of nano pores, and the percolation process is more complicated due to the water. Consider of the nano pore of the coal, the capillary force's effect will be more important. The different pressure will cause different flow channel, which will change the permeability. In this paper, the relative permeability model of coalbed methane reservoir has been built which considers the gas diffusion and slippage effect, pore throat structure parameter, water saturation distribution, and gas water interface pressure drop. It can describe the difference flow channel between different pressure.

1 Preface

There is the huge amount of resources of CBM, the global CBM resources are about 256.1×10^{12} m^3, mainly in the former Soviet Union, North America, and the Asia Pacific region. In 2011, the global coalbed methane production exceeded 700×10^8 m^3 (Birol, 2010). However, due to the characteristics of low porosity, low permeability, complicated pore structure, high capillary pressure, and high initial water content, the coalbed gas flow is very complicated (Marle, 1981). Therefore, the study of gas water permeability curve of coalbed gas reservoir is the basis of gas well productivity and water production evaluation and prediction, and it is of great significance to the efficient and economic development of coalbed methane reservoir (Yang and Wei, 2015).

Relative permeability is an effective tool for studying multiphase fluid flow in porous media. For conventional reservoirs, a relatively reliable relative permeability curve can be obtained by laboratory core test (steady state method or non-steady state method) (Gong *et al.*, 2014). But because of the coalbed gas reservoir permeability is low, the stable steady state method will take a very long time, and the operation is relatively complex. For the non-steady state method, the coalbed gas reservoirs are rich in micro nano pore, which causes the strong heterogeneity and gas is easy to break in through the cracks, it makes non-steady displacement experiment very difficult. Also, the experimental results are greatly affected by human factors and computational methods (Chima and Geiger, 2012; Yang and Wei, 2015). The lattice Boltzmann simulation at the pore scale is another feasible method to obtain the phase permeability curve. However, this method needs a lot of calculation resources and time, which leads to some limitations in practical application (Li *et al.*, 2014; Wu *et al.*, 2015a). Therefore, based on the ideal pore structure and the consideration of different displacement mechanisms, the analytical method not only helps to understand the mechanism of gas water two-phase flow, but also is a convenient and practical method (Wu *et al.*, 2015a, b).

According to the different Knudsen number, which can be calculated by average porous diameter (d) and the mean free path of particle (λ), the formula is $K_n = \lambda/d$. The transmission mechanism of the gas can be divided into continuous flow ($K_n < 10^{-3}$), slip flow ($10^{-3} < K_n < 10^{-1}$),

* Corresponding author: pengzy0328@sina.com

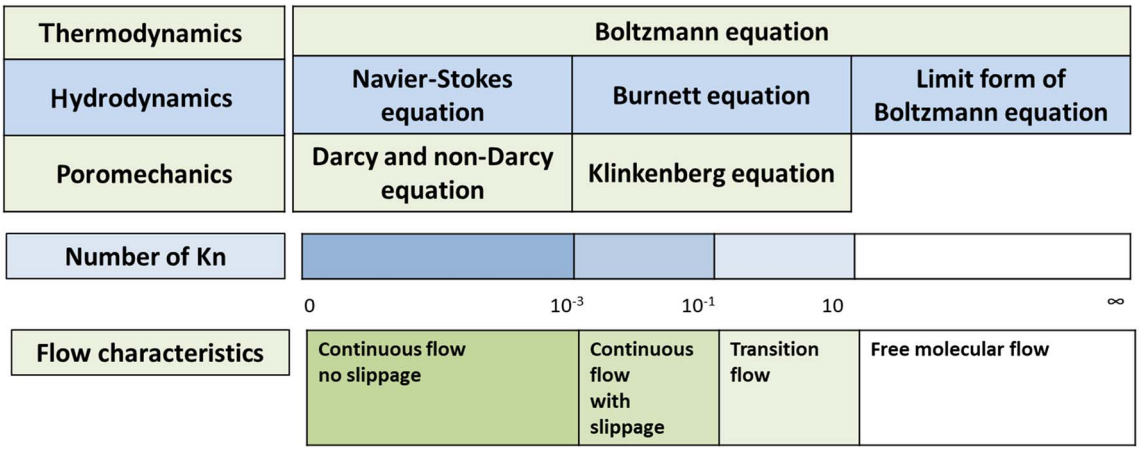

Fig. 1. Knudsen number and gas flow regimes Ertekin *et al.* (1986).

transition flow ($10^{-1} < K_n < 10$) and free molecular flow ($K_n > 10$) (Sampath and Keighim, 1982; Wu *et al.*, 2016a). The Knudsen number of typical coalbed gas reservoir pressure and temperature conditions is near 10^{-1}, therefore, the transmission mechanism comprises a continuous flow and slip flow, and transition flow may be included (Klinkenberg, 1941). Knudsen (1934) defined the ratio of the mean free range of gas molecules to the porous medium scale as the Knudsen number for characterizing the rarefied effects of gases. Then, based on the Knudsen number, Schaaf and Chambré (1961) divided the gas phase nano hole transmission mechanism into four basic types, which is continuous flow, slip flow, transition flow, and Knudsen diffusion. After years of research, the continuous flow, slip flow, and Knudsen diffusion, has formed a relatively complete theoretical system (Fig. 1).

With further research, Ertekin *et al.* (1986) draw lessons from weight factor, interconnection Fick diffusion and Knudsen diffusion. But because of the weight factor will not change with the Knudsen number, the results are quite different from the result from molecular simulation and experimental. Liu *et al.* (2002) given the weight factor's specific expression, while is limited the situation which the Knudsen number must less than 1. The model built by Beskok and Karniadakis (1999) is able to describe all the transport mechanisms known for gas phases in nanoscale pore. But the model has multiple experience factor and cannot degenerate to Knudsen flow model when the Knudsen number is large. Javadpour *et al.* (2007) and Javadpour (2009) linear addition slip flow and Knudsen diffusion based on Maxwell theory to get the transmission model in all Knudsen number. Subsequently, Darabi *et al.* (2012) and Singh *et al.* (2014) revise the model by consider real gas effect, pore wall roughness and so on. Recently, Wu *et al.* (2014) have established the weighting coefficients of diffusion and slippage flow according to the molecular collision theory. The deduced gas flow model can be well fitted with the molecular simulation results. Then further correct the model on the basis of pore shape, pore wall roughness, real gas effect and gas rarefaction effect (Wu *et al.*, 2015c–e, 2016b).

In this paper, the two order slip model and the weight coefficient proposed by Wu *et al.* (2016b) are used to correct the gas free Hagen–Poiseuille equation. Then, established the gas water two phase relative permeability model based on the fractal theory of porous media and capillary bundle model, which considered gas slippage effect, pore roar structure parameter and water saturation distribution. Finally, the correctness of the model is verified by experimental data in public.

2 Model building

Based on the Hagen–Poiseuille continuous equation, two order slip model or no slip condition, introduced the weight coefficients, and the transport model of gas and water in micron scale pore is established by using boundary as coupling condition. This model can take into account the influence of pressure and temperature on fluid transport, and reasonably describe the gas flow behavior in the pore roar of coalbed methane reservoir.

2.1 Single pipe flow model

If the flow of gas and water in the micron pores is laminar, the velocity distribution of the fluid along the pipe diameter still satisfies the continuity equation, if the boundary conditions are properly treated (Cao *et al.*, 2009; Wu, 2008).

Continuity equation of gas:

$$\frac{\mu_g}{r}\frac{\partial v_g}{\partial r}\left(r\frac{\partial v_g}{\partial r}\right)=\frac{\partial p}{\partial z}. \tag{1}$$

Continuity equation of water:

$$\frac{\mu_w}{r}\frac{\partial v_w}{\partial r}\left(r\frac{\partial v_w}{\partial r}\right)=\frac{\partial p}{\partial z}, \tag{2}$$

where v is flow velocity in pore (m/s), r is radial distance from the middle of capillary to any position (m), r_0 is capillary radius (m), μ is aqueous viscosity (Pa · s), p is pressure (Pa), z is distance along the flow equation (m).

Subscript w means aqueous phase, while subscript g means gas phase.

Owing to the kinetic energy transfer in the gas–solid near wall is affected by the molecules interaction between gases and gases, or gases and walls. The gas molecules on the wall do not completely adhere to the wall, which is called the gas slip. When the number of Knudsen gas increased to 10^{-3}, its influence on the gas transmission cannot be ignored (Sampath and Keighim, 1982; Wu *et al.*, 2016b). When the Knudsen number is less than 10^{-1}, the wall slip velocity can be characterized by the two order slip model (Tocci *et al.*, 2016):

$$v_s = C_1\lambda\frac{\partial v_g}{\partial r} - C_2\lambda^2\frac{\partial^2 v_g}{\partial r^2}\bigg|_{r=r_0}, \tag{3}$$

where C_1 and C_2 are first order slip factor and second slip factor, which often valued as 4/3 and 1/4 (Tocci *et al.*, 2016; Wu *et al.* 2017). λ is mean free path of gas molecules, which can be calculated by the follows:

$$\lambda = \frac{k_b T}{\sqrt{2}\pi d^2 p_{\text{ave}}}, \tag{4}$$

where k_b is Boltzmann's constant, T is absolute temperature, d is molecular diameter of methane, P_{ave} is average pressure of capillary inlet and outlet.

Due to the smaller pore size in the actual coalbed methane reservoir, the transition flow of $10^{-1} < K_n < 10$ cannot be neglected. Therefore, based on the weight coefficient of Wu *et al.* (2015d), superposition the continuous flow and Knudsen diffusion of gas, correct the flow of gas in the pores:

$$J_{T-\text{tube}} = f_{\text{slip}-\text{tube}}J_{\text{slip}-\text{tube}} + f_{K_n-\text{tube}}J_{K_n-\text{tube}}, \tag{5}$$

where $J_{T\text{-tube}}$ is total mass flow (kg/m^2 · s), $J_{\text{slip–tube}}$ is mass flow at slip flow (kg/m^2 · s), $J_{K_n-\text{tube}}$ is mass flow at Knudsen diffusion (kg/m^2 · s), $f_{\text{slip–tube}}$ and $f_{K_n-\text{tube}}$ are weight coefficient of slip flow and Knudsen diffusion, which can be calculated by the follows (Wu *et al.*, 2015a, b):

$$f_{\text{slip}-\text{tube}} = \frac{\omega_{m-m}}{\omega_{m-w}+\omega_{m-m}} = \frac{1}{1+K_n}, \tag{6}$$

$$f_{K_n-\text{tube}} = \frac{\omega_{m-w}}{\omega_{m-w}+\omega_{m-m}} = \frac{1}{1+1/K_n}, \tag{7}$$

where ω_{m-m} is collision frequency between molecules and molecules, which depends on pore volume or cross-sectional area. And ω_{m-w} is collision frequency between molecules and walls, which depends on pore surface area or perimeter.

For the boundary conditions of single-phase water flow, because of the strong force of water molecules and solid molecules, the boundary effect of single-phase flow is usually less than 1 nm (Katz and Thompson, 1985; Yu and Liu, 2004), which can be ignored. Therefore, it can be considered that the velocity of water molecules at the wall surface is 0, and the wall effect has no effect on the water transmission, which means single-phase water flow can be characterized by the non-slip boundary conditions. So, the boundary conditions of single-phase gas and single-phase water flow can be expressed as follows (Fig. 2):

$$\frac{\partial v_g}{\partial r}(r = r_o) = 0, \tag{8}$$

$$v_g\big|_{r=r_0} = v_w\big|_{r=r_0} + v_s\big|_{r=r_0}, \tag{9}$$

$$\frac{\partial v_w}{\partial r}(r = r_o) = 0, \tag{10}$$

$$v_w\big|_{r=r_0} = 0, \tag{11}$$

Integral equations (1) and (2), the flow equation of gas phase and aqueous phase can be obtained as follows:

$$q_g = f_{K_n}\frac{\nabla p}{L}\frac{\pi}{8\mu_g}r_0^4 + f_{\text{slip}}\frac{\nabla p}{L} \times \frac{\pi}{8\mu_g}\left(4C_1\lambda r_0^3 - 4C_2\lambda^2 r_0^2\right), \tag{12}$$

$$q_w = \frac{\nabla p}{L}\frac{\pi}{8\mu_w}r_0^4, \tag{13}$$

equation (11) is flow equation with boundary slip, while equation (12) is the classical Hagen–Poiseuille equation with no slip.

2.2 Relative permeability model

2.2.1 *Fractal theory*

From the macroscopic scale to the microscopic scale, a large number of porous media in nature exhibit fractal and self similar characteristics (Majumdar and Bhushan, 1990; Yu and Li, 2011). According to the fractal theory, the cumulative pore size distribution can be expressed as follows (Yu and Cheng, 2002):

$$N(\varepsilon > r) = \left(\frac{r_{\max}}{r}\right)^{D_f}, \tag{14}$$

where N is number of pores, ε is length scale (m), r and $r_{\max}$ are aperture and maximum aperture (m), D_f is fractal dimension of pore size distribution, the ranges of 2D and 3D holes are $0 < D_f < 2$, and it can be calculated as follows (Bonnet *et al.*, 2001):

$$D_f = d - \frac{\ln\varphi}{\ln(r_{\min}/r_{\max})}, \tag{15}$$

where d is Euclidean space, equals 2 or 3, in this work, $d = 2$ has been used because the capillary can be regarded as 2D, $r_{\min}$ is the minimum aperture (m), φ is porosity.

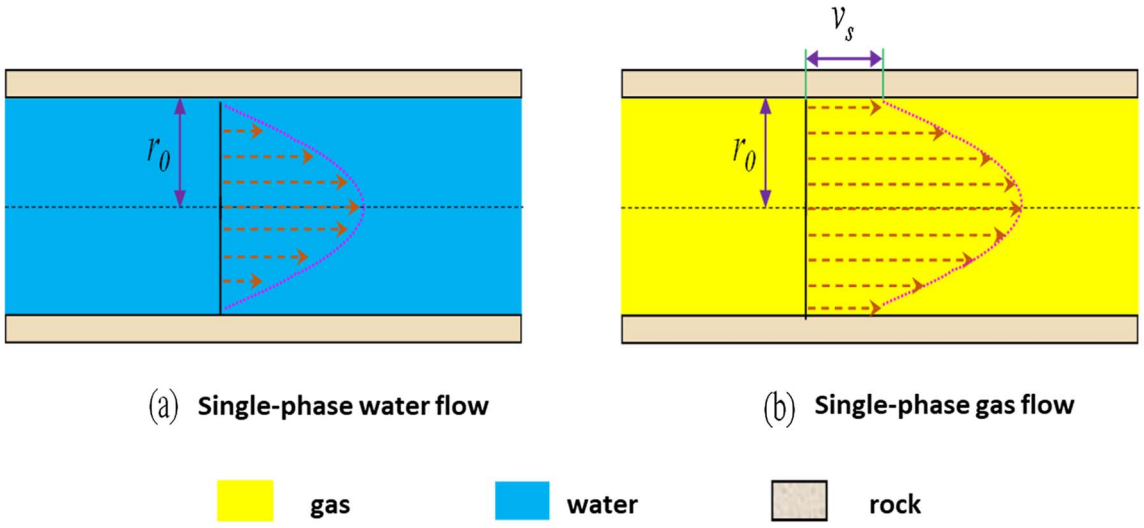

Fig. 2. Velocity distribution along the circular microtube of single gas/water flow.

Total pore number between the maximum aperture and the minimum aperture can be calculated as follows:

$$N = \left(\frac{r_{\max}}{r_{\min}}\right)^{D_f}. \tag{16}$$

The distribution probability density function of pores with different sizes can be calculated as follows (Xu and Yu, 2008):

$$f(r) = D_f r_{\min}^{D_f} r^{-(D_f+1)}. \tag{17}$$

Considering the actual pore in the matrix is tortuous, continuous characterization unit of porous media (REV) with characteristic length L_0, the actual length of the capillary will be L, and the L can be calculated as follows (Xu *et al.*, 2013):

$$L(r) = (2r)^{1-D_T} L_0^{D_T}, \tag{18}$$

where D_T is the tortuosity fractal dimension, the range of 2D and 3D are $1 < D_T < 2$ and $1 < D_T < 3$. $D_T = 1$ means a straight capillary, $D_T = 2$ (in 2D) or 3 (in 3D) means the capillary is infinite tortuosity and can fill the whole space (Burdine, 1953). D_T can be calculated as follows:

$$D_T = 1 + \frac{\ln \tau_{\text{ave}}}{\ln(L_0/2r_{\text{ave}})}, \tag{19}$$

where the parameter τ_{ave} and $L_0/2r_{\text{ave}}$ can be calculated as follows:

$$\tau_{\text{ave}} = \frac{1}{2}\left[1 + \frac{1}{2}\sqrt{1-\varphi} + \sqrt{1-\varphi}\,\frac{\sqrt{\left(\frac{1}{\sqrt{1-\varphi}} - 1\right)^2 + \frac{1}{4}}}{1-\sqrt{1-\varphi}}\right], \tag{20}$$

$$\frac{L_0}{2r_{\text{ave}}} = \frac{D_f - 1}{D_f^{1/2}}\left[\frac{1-\varphi}{\varphi}\,\frac{\pi}{4(2-D_f)}\right]^{1/2}\frac{r_{\max}}{r_{\min}}. \tag{21}$$

Use the porosity φ, and the result of equation (15), the necessary parameter of equation (19) can be calculated by equations (20) and (21), which means the D_T can be calculated by equation (19). Then, the relationship between characteristic length L_0 and actual length of the capillary L is shown by equation (18).

2.2.2 Relative permeability model

In order to simplify the model, the complicated pore structure in coalbed methane reservoir is simplified as the capillary bundle model, which consists of some unequal tortuous capillary, which are vertical to REV. The fluid flows only from the capillary bundle, and the circumferential aspect of REV has no fluid flow, which is shown by Figure 3. The pore size distribution and flow tortuosity of capillary bundle model is satisfied with the fractal theory which is shown by equations (14)–(21) (Kim *et al.*, 2012).

A large amount of adsorbed gas and free gas in the coal reservoir are stored in nanometer pores, while a lot of research in coal geology shows that the nanometer pores in coal reservoir are mainly gas pore, which is formed by gas production during coalification. And the other nano pores are not the main pores because of their small number or poor connectivity (Zhang, 2016). On the other hand, it is difficult for water molecules to enter the nano pores of coal because of the surface hydrophobic effect of organic matter (Firouzi *et al.*, 2014). So suppose there is a critical capillary radius r_c, the capillary which the aperture less than r_c is full of single-phase gas, while the capillary which the aperture larger than r_c may be full of single-phase gas or single-phase water. And the capillary which the aperture less than r_c are randomly connected.

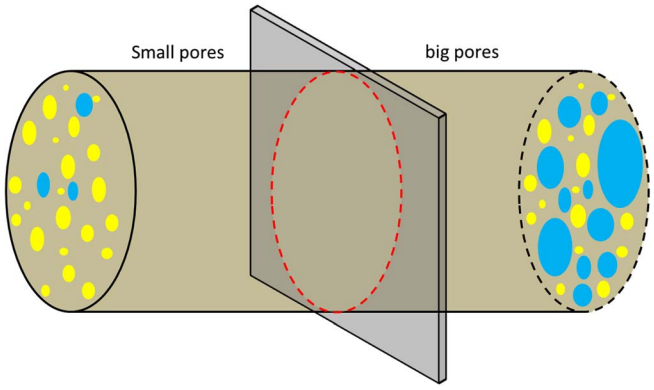

Fig. 3. Physical conceptual model of gas/water flow pattern in tight sandstone sample.

Based on the above hypothesis, the capillary connection can be divided into two categories, the gas capillary which the aperture less than r_c connected with the gas capillary which the aperture larger than r_c, and with the water capillary which the aperture larger than r_c. The proportion of the gas capillary connect gas capillary to total capillary is α_1, while the proportion of the gas capillary connect water capillary to total capillary is α_2:

$$\alpha_1 = \frac{1 - S_w - \dfrac{\int_{r_{\min}}^{r_c} \pi r^2 f(r)\mathrm{d}r}{\int_{r_{\min}}^{r_{\max}} \pi r^2 f(r)\mathrm{d}r}}{1 - \dfrac{\int_{r_{\min}}^{r_c} \pi r^2 f(r)\mathrm{d}r}{\int_{r_{\min}}^{r_{\max}} \pi r^2 f(r)\mathrm{d}r}} = \frac{1 - S_w - (r_c^{-D_f} - r_{\min}^{-D_f})/(r_{\max}^{-D_f} - r_{\min}^{-D_f})}{1 - (r_c^{-D_f} - r_{\min}^{-D_f})/(r_{\max}^{-D_f} - r_{\min}^{-D_f})},$$

$$\alpha_2 = \frac{S_w}{1 - \dfrac{\int_{r_{\min}}^{r_c} \pi r^2 f(r)\mathrm{d}r}{\int_{r_{\min}}^{r_{\max}} \pi r^2 f(r)\mathrm{d}r}} = \frac{S_w}{1 - (r_c^{-D_f} - r_{\min}^{-D_f})/(r_{\max}^{-D_f} - r_{\min}^{-D_f})},$$

where S_w is water saturation in matrix. Consider the influence of tortuosity and pressure, single tube flow formula of gas and water (12) and (13) can be reduced as follows:

$$q_g = f_{K_n} \frac{\nabla p}{L(r)} \frac{\pi}{8\mu_g} r_0^4 + f_{\text{slip}} \frac{\nabla p}{L(r)} \times \frac{\pi}{8\mu_g} \left(4C_1 \lambda r_0^3 - 4C_2 \lambda^2 r_0^2\right), \tag{22}$$

$$q_w = \frac{\nabla p}{L(r)} \frac{\pi}{8\mu_w} r_0^4, \tag{23}$$

where $L(r)$ is the actual length of the pore path, $\nabla p_g/L$ and $\nabla p_w/L$ are pressure gradient of gas and water.

Integral equation (22), for the gas phase flow into the water phase, only the capillary force is less than pressure gradient can be migrated. Gas volume flow of REV can be shown as follows:

See equation (24) *below.*

where the r_p is the minimum capillary radius that can be displaced at present pressure, which can be calculated as follows:

$$r_p = \frac{2\sigma}{\nabla p}.$$

Similarly, integral equation (23), water volume flow of REV can be shown as follows:

$$Q_w = N \int_{r_c}^{r_{\max}} q_w f(r)\mathrm{d}r = \pi D_f r_{\min}^{D_f} \frac{\nabla p_w}{2^{4-D_T} L_0^{D_T} \mu_g} \left(\frac{r_{\max}^{D_T - D_f + 3} - r_c^{D_T - D_f + 3}}{D_T - D_f + 3} \right). \tag{25}$$

On the other hand, the flow of gas and water can also be expressed by Darcy's expansion formula:

$$Q_g = -\frac{K_g}{\mu_g} \frac{A}{(1 - S_w)} \frac{\nabla p_g}{L_0}, \tag{26}$$

$$\begin{aligned} Q_g &= \alpha_1 N \int_{r_c}^{r_{\max}} q_g f(r)\mathrm{d}r + \alpha_2 N \int_{r_p}^{r_{\max}} q_g f(r)\mathrm{d}r \\ &= \alpha_1 \pi D_f r_{\min}^{D_f} \\ &\quad \times \frac{\nabla p_g}{2^{4-D_T} L_0^{D_T} \mu_g} \left(\frac{r_{\max}^{D_T - D_f + 3} - r_c^{D_T - D_f + 3}}{D_T - D_f + 3} f_{K_n} + \frac{r_{\max}^{D_T - D_f + 2} - r_c^{D_T - D_f + 2}}{D_T - D_f + 2} 4C_1 f_{\text{slip}} \lambda - \frac{r_{\max}^{D_T - D_f + 1} - r_c^{D_T - D_f + 1}}{D_T - D_f + 1} 4C_2 f_{\text{slip}} \lambda^2 \right) \\ &\quad + \alpha_2 \pi D_f r_{\min}^{D_f} \\ &\quad \times \frac{\nabla p_g - \nabla p_c}{(2^{4-D_T} L_0^{D_T} \mu_g) \nabla p_g} \left(\frac{r_{\max}^{D_T - D_f + 3} - r_p^{D_T - D_f + 3}}{D_T - D_f + 3} f_{K_n} + \frac{r_{\max}^{D_T - D_f + 2} - r_p^{D_T - D_f + 2}}{D_T - D_f + 2} 4C_1 f_{\text{slip}} \lambda - \frac{r_{\max}^{D_T - D_f + 1} - r_p^{D_T - D_f + 1}}{D_T - D_f + 1} 4C_2 f_{\text{slip}} \lambda^2 \right), \end{aligned} \tag{24}$$

$$Q_w = -\frac{K_w}{\mu_w}\frac{A}{S_w}\frac{\nabla p_w}{L_0}, \tag{27}$$

where K_g and K_w are effective permeability of gas and water.

See equation (28) *below.*

Solve the equations (24)–(27), the effective permeability of gas and water can be shown as follows:

$$K_w = -S_w\frac{\varphi}{1-\varphi}r_{\min}^{D_f-2}\frac{2-D_f}{2^{4-D_f}L_0^{D_T-1}} \times \frac{r_{\max}^{D_T-D_f+3}-r_c^{D_T-D_f+3}}{D_T-D_f+3}. \tag{29}$$

Bring $S_w = 1$ into equation (29), the absolute permeability of coal can be shown as follows:

$$K = -\frac{\varphi}{1-\varphi}r_{\min}^{D_f-2}\frac{2-D_f}{2^{4-D_f}L_0^{D_T-1}}\frac{r_{\max}^{D_T-D_f+3}-r_{\min}^{D_T-D_f+3}}{D_T-D_f+3}. \tag{30}$$

So, relative permeability of gas and water can be shown as follows:

See equation (31) *below.*

$$K_{rw} = S_w\frac{r_{\max}^{D_T-D_f+3}-r_c^{D_T-D_f+3}}{r_{\max}^{D_T-D_f+3}-r_{\min}^{D_T-D_f+3}}. \tag{32}$$

3 Model verification and discussion

3.1 Model verification

This paper proving the reliability of the model by using two sets of different test data of gas water relative permeability in published papers (Zhang *et al.*, 2017). Two test coal's porosity in the literature is 9.1% and 8.6%, while the maximum and minimum aperture are $r_{\max} = 100$ μm, $r_{\min} = 0.001$ μm. Fractal dimension of pore size distribution D_f and the tortuosity fractal dimension D_T are calculated by equations (14), (19), and (20). The pressure is 2 MPa and 6 MPa.

A conclusion from the comparison results, the model established in this paper by equations (31) and (32) can be better fitted with the experimental data as Figure 4. For the high pressure reservoir, the model is more accurate than other model. Because of the effect of slippage and capillary force have been considered in this model, which is shown by Figure 5.

The model's deviation can be calculated by the following. The result of both effect is shown (Tabs. 1 and 2):

$$\delta = (k_{\text{experiment}} - k_{\text{model}})^2. \tag{33}$$

From the calculation results, it can be seen that the model has high fitting accuracy for both high pressure and low pressure.

3.2 Discussion

Using the new model to calculate the gas relative permeability in different pressure by the same properties in Section 3.1, the result is shown as Figure 6.

$$K_g = -(1-S_w)\frac{\varphi}{1-\varphi}r_{\min}^{D_f-2}\frac{2-D_f}{2^{4-D_f}L_0^{D_T-1}} \times \left[\left(\frac{r_{\max}^{D_T-D_f+3}-r_c^{D_T-D_f+3}}{D_T-D_f+3}f_{K_n} + \frac{r_{\max}^{D_T-D_f+2}-r_c^{D_T-D_f+2}}{D_T-D_f+2}4C_1f_{\text{slip}}\lambda - \frac{r_{\max}^{D_T-D_f+1}-r_c^{D_T-D_f+1}}{D_T-D_f+1}4C_2f_{\text{slip}}\lambda^2\right)\alpha_1 + \frac{\nabla p_w-\nabla p_c}{\nabla p_w}\left(\frac{r_{\max}^{D_T-D_f+3}-r_p^{D_T-D_f+3}}{D_T-D_f+3}f_{K_n} + \frac{r_{\max}^{D_T-D_f+2}-r_p^{D_T-D_f+2}}{D_T-D_f+2}4C_1f_{\text{slip}}\lambda - \frac{r_{\max}^{D_T-D_f+1}-r_p^{D_T-D_f+1}}{D_T-D_f+1}4C_2f_{\text{slip}}\lambda^2\right)\alpha_2\right], \tag{28}$$

$$K_{rg} = (1-S_w)\left[\left(\frac{r_{\max}^{D_T-D_f+3}-r_c^{D_T-D_f+3}}{r_{\max}^{D_T-D_f+3}-r_{\min}^{D_T-D_f+3}}f_{K_n} + \frac{D_T-D_f+3}{D_T-D_f+2}\frac{r_{\max}^{D_T-D_f+2}-r_c^{D_T-D_f+2}}{r_{\max}^{D_T-D_f+3}-r_{\min}^{D_T-D_f+3}}4C_1f_{\text{slip}}\lambda - \frac{D_T-D_f+3}{D_T-D_f+1}\frac{r_{\max}^{D_T-D_f+1}-r_c^{D_T-D_f+1}}{r_{\max}^{D_T-D_f+3}-r_{\min}^{D_T-D_f+3}}4C_2f_{\text{slip}}\lambda^2\right)\alpha_1 + \frac{\nabla p_w-\nabla p_c}{\nabla p_w}\left(\frac{r_{\max}^{D_T-D_f+3}-r_p^{D_T-D_f+3}}{r_{\max}^{D_T-D_f+3}-r_{\min}^{D_T-D_f+3}}f_{K_n} + \frac{D_T-D_f+3}{D_T-D_f+2}\frac{r_{\max}^{D_T-D_f+2}-r_p^{D_T-D_f+2}}{r_{\max}^{D_T-D_f+3}-r_{\min}^{D_T-D_f+3}}4C_1f_{\text{slip}}\lambda - \frac{D_T-D_f+3}{D_T-D_f+1}\frac{r_{\max}^{D_T-D_f+1}-r_p^{D_T-D_f+1}}{r_{\max}^{D_T-D_f+3}-r_{\min}^{D_T-D_f+3}}4C_2f_{\text{slip}}\lambda^2\right)\alpha_2\right], \tag{31}$$

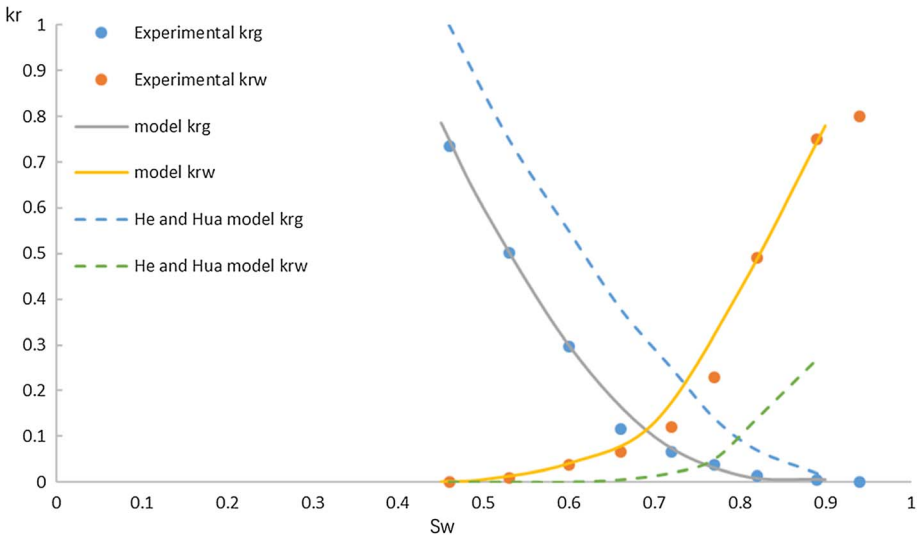

Fig. 4. Different model and experimental data in 2 MPa.

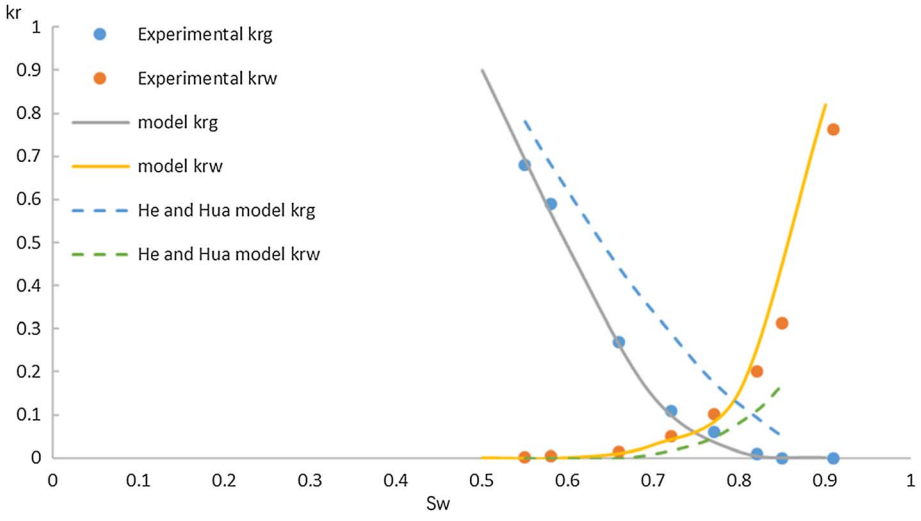

Fig. 5. Different model and experimental data in 6 MPa.

Table 1. Different model's deviation in 2 MPa.

	Experimental data		He and Hua model				This model			
S_w	k_{rg}	k_{rw}	k_{rg}	k_{rw}	k_{rg} deviation	k_{rw} deviation	k_{rg}	k_{rw}	k_{rg} deviation	k_{rw} deviation
0.46	0.73	0	1	0	0.07	0	0.73	0	6.15E-08	0
0.53	0.50	0.01	0.75	0	0.062	0.0001	0.49	0.013	2.63E-05	0.000009
0.6	0.29	0.04	0.55	0	0.064	0.001	0.29	0.03	1.17E-06	0.000016
0.66	0.11	0.066	0.38	0.005	0.07	0.003	0.16	0.07	0.002	1.37E-05
0.72	0.06	0.12	0.25	0.02	0.03	0.01	0.07	0.17	7.22E-06	0.002714
0.77	0.037	0.23	0.14	0.05	0.011	0.03	0.027	0.32	0.0001	0.0081
0.82	0.013	0.49	0.07	0.14	0.003	0.12	0.005	0.48	6.83E-05	4.23E-05
0.89	0.0053	0.75	0.02	0.27	0.0002	0.23	0.002	0.75	1.09E-05	0.000025
				Average	0.039	0.05		Average	0.0003	0.001

Table 2. Different model's deviation in 6 MPa.

	Experimental data		He and Hua model				This model			
S_w	k_{rg}	k_{rw}	k_{rg}	k_{rw}	k_{rg} deviation	k_{rw} deviation	k_{rg}	k_{rw}	k_{rg} deviation	k_{rw} deviation
0.55	0.68	0.002	0.78	0	0.01	0.000004	0.69	0	1E-04	0.000004
0.58	0.59	0.005	0.68	0	0.008	0.00003	0.57	0	0.0004	0.00002
0.66	0.27	0.013	0.44	0	0.03	0.0002	0.26	0.009	0.0001	0.00002
0.72	0.11	0.051	0.29	0.02	0.03	0.001	0.1	0.04	1E-04	0.00006
0.77	0.06	0.102	0.18	0.05	0.01	0.003	0.04	0.08	0.0004	0.0004
0.82	0.01	0.2	0.09	0.11	0.007	0.008	0.007	0.24	0.000009	0.001
0.85	0	0.31	0.05	0.17	0.003	0.02	0.002	0.44	3.24E-06	0.02
0.91	0	0.76	0.02	0.33	0.0003	0.19	0	0.86	0	0.009
				Average	0.01	0.02		Average	0.0001	0.003

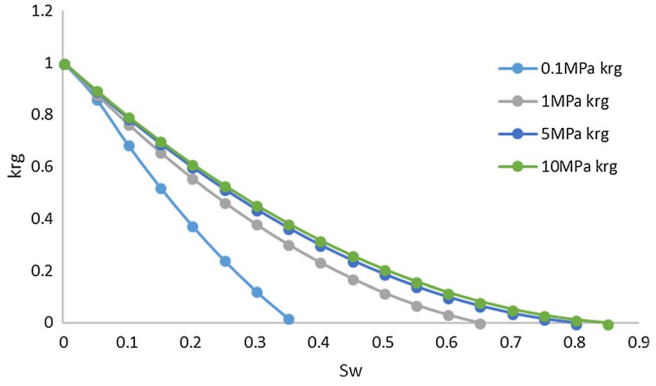

Fig. 6. Gas relative permeability in different pressure.

With the increase of pressure, the gas relative permeability increase fast in lower pressure, while changes a little when the pressure is larger than 5 MPa. This is because with the increase of pressure, the more nano pore can be flown by fluid, but when the pressure is larger than 5 MPa, the pressure is larger than most pores capillary pressure, the effect of pressure will become very small.

But because of the model has been using fractal theory to describe the pore characteristic, which means the pores distribution of different sizes is very regular, which cause the relative permeability in different pressure is very similar, that will cause some error. If there were some more accurate method to describe pore distribution, this method will have higher precision.

4 Conclusion

Based on the Hagen–Poiseuille continuous equation with two order slip model, introduced the weight coefficients and fractal theory, considered the distribution of gas and water, established a gas-water relative permeability model of coalbed methane reservoir, and the transport model of gas and water in micron scale pore is established by using boundary as coupling condition. This model can take into account the influence of pressure and temperature on fluid transport, and reasonably describe the gas flow behavior in the pore roar of coalbed methane reservoir which has been validated by published experimental data of gas water relative permeability, and can be used to describe the fluid flow behavior in micro scale pores of coalbed methane reservoirs.

References

Beskok A., Karniadakis G.E. (1999) Report: A model for flows in channels, pipes, and ducts at micro and nano scales, *Nanoscale Microscale Therm. Eng.* **3**, 1, 43–77. doi: 10.1080/108939599199864.

Birol F. (2010) *World energy outlook 2010*, International Energy Agency, Washington, DC.

Bonnet E., Bour O., Odling N.E., Davy P., Main I., Cowie P., Berkowitz B. (2001) Scaling of fracture systems in geological media, *Rev. Geophys.* **39**, 3, 347–383. doi: 10.1029/1999rg000074.

Burdine N.T. (1953) Relative permeability calculations from pore size distribution data, *J. Pet. Technol.* **5**, 3, 71–78. doi: 10.2118/225-g.

Cao B.Y., Sun J., Chen M., Zeng Y. (2009) Molecular momentum transport at fluid-solid interfaces in MEMS/NEMS: A review, *Int. J. Mol. Sci.* **10**, 11, 4638. doi: 10.3390/ijms10114638.

Chima A., Geiger S. (2012) An analytical equation to predict gas/water relative permeability curves in fractures, in: *The Annual Meeting for the SPE Latin America and Caribbean Petroleum Engineering Conference*, 16–18 April, Mexico City.

Darabi H., Ettehad A., Javadpour F., Sepehrnoorl K. (2012) Gas flow in ultra-tight shale strata, *J. Fluid Mech.* **710**, 12, 641–658. doi: 10.1017/jfm.2012.424.

Ertekin T., King G.R., Schwerer F.C. (1986) Dynamic gas slippage: A unique dual-mechanism approach to the flow of gas in tight formations, *SPE Form. Eval.* **1**, 1, 43–52. doi: 10.2118/12045-pa.

Firouzi M., Rupp E.C., Liu C.W., Wilcox J. (2014) Molecular simulation and experimental characterization of the nanoporous structures of coal and gas shale, *Int. J. Coal Geol.* **121**, 1, 123–128. doi: 10.1016/j.coal.2013.11.003.

Gong B., Liu X., Qin G. (2014) A Lattice Boltzmann model for multi-component vapor-liquid two phase flow, *Petrol. Explor. Dev.* **41**, 5, 695–702. doi: 10.11698/PED.2014.05.17.

Javadpour F. (2009) Nanopores and apparent permeability of gas flow in mudrocks (Shales and Siltstone), *J. Can. Pet. Technol.* **48**, 8, 16–21. doi: 10.2118/09-08-16-da.

Javadpour F., Fisher D., Unsworth M. (2007) Nanoscale gas flow in shale gas sediments, *J. Can. Pet. Technol.* **46**, 10, 55–61. doi: 10.2118/07-10-06.

Katz A.J., Thompson A.H. (1985) Fractal sandstone pores: Implications for conductivity and pore formation, *Phys. Rev. Lett.* **54**, 12, 1325–1328. doi: 10.1103/physrevlett.54.1325.

Kim T.W., Tokunaga T.K., Shuman D.B., Stephen R.S., Matt N., Lanzirotti A. (2012) Thickness measurements of nanoscale brine films on silica surfaces under geologic CO_2 sequestration conditions using synchrotron X-ray fluorescence, *Water Resour. Res.* **48**, 9. doi: 10.1029/2012wr012200.

Klinkenberg L.J. (1941) The permeability of porous media to liquids and gases, *SOCAR Proc.* **2**, 2, 200–213. doi: 10.5510/ogp20120200114.

Knudsen M. (1934) Die Gesetze der Molekularströmung und der inneren Reibungsströmung der Gase durch Röhren, *Ann. Phys.* **333**, 1, 75–130. doi: 10.1002/andp.19093330106.

Li Y., Li X., Teng S., Xu D. (2014) Improved models to predict gas–water relative permeability in fractures and porous media, *J. Nat. Gas Sci. Eng.* **19**, 7, 190–201. doi: 10.1016/j.jngse.2014.05.006.

Liu Q., Shen P., Yang P. (2002) Pore scale network modelling of gas slippage in tight porous media, *Contemp. Math.* **295**, 367–375. doi: 10.1090/conm/295/05027.

Majumdar A.A., Bhushan B. (1990) Role of fractal geometry in roughness characterization and contact mechanics of surfaces, *ASME J. Tribol.* **112**, 2, 205–216. doi: 10.1115/1.2920243.

Marle C. (1981) *Multiphase flow in porous media*, Éditions Technip, France.

Sampath K., Keighim C.W. (1982) Factors affecting gas slippage in tight sandstones of cretaceous age in the Uinta Basin, *J. Pet. Technol.* **34**, 11, 2715–2720. doi: 10.2118/9872-pa.

Schaaf S.A., Chambré P.L. (1961) *Flow of rarefied gases*, Princeton University Press, Princeton.

Singh H., Javadpour F., Ettehadtavakkol A., Darabi H. (2014) Nonempirical Apparent Permeability of Shale, *SPE Reserv. Evalu. Eng.* **17**, 3, 414–424. doi: 10.2118/170243-pa.

Tocci G., Joly L., Michaelides A. (2016) Friction of water on graphene and hexagonal boron nitride from *ab initio* methods: Very different slippage despite very similar interface structures, *Nano Lett.* **14**, 12, 6872–6877. doi: 10.1021/nl502837d.

Wu L. (2008) A slip model for rarefied gas flows at arbitrary Knudsen number, *Appl. Phys. Lett.* **93**, 25, 253103. doi: 10.1063/1.3052923.

Wu K., Li X., Wang C., Yu W., Guo C., Ji D., Ren G., Chen Z. (2014) Apparent permeability for gas flow in shale reservoirs coupling effects of gas diffusion and desorption, in: *The Annual Meeting for the Unconventional Resources Technology Conference, 25–27 August, Denver.*

Wu K., Li X., Chen Z. (2015a) The mechanism and mathematical model for the adsorbed gas surface diffusion in nanopores of shale gas reservoirs, *Sci. Sin. Technol.* **45**, 5, 525–540. doi: 10.1360/n092014-00263.

Wu K., Li X., Chen Z. (2015b) A model for gas transport through nanopores of shale gas reservoirs, *Acta Petrol. Sin.* **36**, 7, 837–848.

Wu K., Chen Z., Li X. (2015c) Real gas transport through nanopores of varying cross-section type and shape in shale gas reservoirs, *Chem. Eng. J.* **281**, 813–825. doi: 10.2118/175453-ms.

Wu K., Li X., Wang C., Chen Z., Yu W. (2015d) A model for gas transport in microfractures of shale and tight gas reservoirs, *AIChE J.* **61**, 6, 2079–2088. doi: 10.1002/aic.14791.

Wu K., Li X., Wang C., Yu W., Chen Z. (2015e) Model for surface diffusion of adsorbed gas in nanopores of shale gas reservoirs, *Ind. Eng. Chem. Res.* **54**, 12, 3225–3236. doi: 10.4043/25662-ms.

Wu K., Li X., Chen Z. (2016a) Real gas transport through nanopores of shale gas reservoirs, *Sci. Sin. Technol.* **46**, 1, 68–78. doi: 10.2118/180086-ms.

Wu K., Chen Z., Li X., Guo C., Wei M. (2016b) A model for multiple transport mechanisms through nanopores of shale gas reservoirs with real gas effect–adsorption-mechanic coupling, *Int. J. Heat Mass Transfer* **93**, 408–426. doi: 10.2118/173201-ms.

Wu K., Chen Z., Li J., Li X., Xu J., Dong X. (2017) Wettability effect on nanoconfined water flow, *Proc. Nat. Acad. Sci. USA* **114**, 13, 3358–3363. doi: 10.1016/j.nantod.2017.05.001.

Xu P., Yu B. (2008) Developing a new form of permeability and Kozeny-Carman constant for homogeneous porous media by means of fractal geometry, *Adv. Water Res.* **31**, 1, 74–81. doi: 10.1016/j.advwatres.2007.06.003.

Xu P., Qiu S., Yu B. (2013) Prediction of relative permeability in unsaturated porous media with a fractal approach, *Int. J. Heat Mass Transfer* **64**, 3, 829–837. doi: 10.1021/ef3013322.

Yang S., Wei J. (2015) *Reservoir physics*, Petroleum Industry Press, Beijing.

Yu B., Cheng P. (2002) A fractal permeability model for bi-dispersed porous media, *Int. J. Heat Mass Transfer* **45**, 14, 2983–2993. doi: 10.1016/s0017-9310(02)00014-5.

Yu B., Li J. (2011) Some fractal characters of porous media, *Fractals* **9**, 3, 365–372. doi: 10.1142/s0218348x01000804.

Yu B., Liu W. (2004) Fractal analysis of permeabilities for porous media, *AIChE J.* **50**, 1, 46–57. doi: 10.1002/aic.10004.

Zhang H. (2016) *A scanning electron microscopic study of unconventional oil and gas reservoir*, Geology Publishing House, Beijing.

Zhang X., Wu C., Liu S. (2017) Characteristic analysis and fractal model of the gas-water relative permeability of coal under different confining pressures, *J. Pet. Sci. Eng.* **159**, 488–496. doi: 10.1016/j.petrol.2017.09.057.